Low-energy electron scattering of NO: *Ab initio* analysis of the $^3\Sigma^-$, $^1\Delta$, and $^1\Sigma^+$ shape resonances in the local complex potential model

Zhiyong Zhang,[1] Wim Vanroose,[1] C. W. McCurdy,[1,2,3] A. E. Orel,[2] and T. N. Rescigno[1]
[1]*Chemical Science, Lawrence Berkeley National Laboratory, Berkeley, California 94720, USA*
[2]*Department of Applied Science, University of California, Davis, California 95616, USA*
[3]*Department of Chemistry, University of California, Berkeley, California 94720, USA*
(Received 21 January 2004; published 14 June 2004)

We present an *ab initio* study of elastic scattering and vibrational excitation of NO by low-energy (0–2.0 eV) electron impact. The low-energy scattering cross sections are dominated by shape resonance contributions associated with the $^3\Sigma^-$, $^1\Delta$, and $^1\Sigma^+$ states of NO^-. Resonance parameters for the three anion states were extracted from an analysis of fixed-nuclei variational (complex Kohn) calculations that employed elaborate trial wave functions. Independent estimates of the resonance parameters were obtained by analytically continuing the results of large-scale coupled-cluster calculations into the plane of complex momentum. The local complex potential model was used to calculate vibrational excitation cross sections, as well as the resonant portion of the vibrationally elastic cross sections. These results were combined with background contributions from the fixed-nuclei calculations to compute elastic and grand total cross sections. Our results capture the essential features of recent measurements of the cross sections, but suggest the need at lower energies for a more sophisticated, nonlocal treatment of nuclear dynamics.

DOI: 10.1103/PhysRevA.69.062711 PACS number(s): 34.80.Gs

I. INTRODUCTION

The diatomic molecule nitric oxide plays an important role in a number of physical, chemical and biological processes. Our interest here is in its interaction with low-energy electrons, which is of direct relevance to understanding its role in various atmospheric processes. The low-energy behavior of e^--NO cross sections has been the focus of several experimental studies [1–4], including three recent investigations [5–7] which have provided absolute values for total, elastic and vibrational excitation cross sections. By contrast, there has been very little theoretical work on electron-NO scattering, especially in the region below 3 eV collision energy which is dominated by negative ion resonances. Several early studies [8,9] provided semiempirical determinations of the resonance parameters obtained from analyses of available experimental data. Tennyson and Noble [10] later performed *R*-matrix calculations, but only at a single internuclear distance, and reported energy-dependent eigenphase sums, but no cross sections. Da Paixao, Lima, and McKoy [11] also performed fixed-nuclei calculations at the equilibrium geometry, but did not report cross sections below 5 eV collision energy. To our knowledge, there have been no previous theoretical estimates of electron-NO cross sections in the important low-energy region below 3 eV.

Low-energy electron-NO scattering poses significant theoretical challenges. Neutral NO is an open-shell molecule with a $^2\Pi$ ground electronic state. The ground state of the negative ion NO^- is a $^3\Sigma^-$ state and is bound by only 24 meV [12]. By analogy with its isoelectronic counterpart O_2, NO^- has low-lying excited states of $^1\Delta$ and $^1\Sigma$ symmetry. All three anion states are electronically unbound at the equilibrium internuclear distance of the neutral and give rise to a rich series of overlapping resonance structures which dominate the electron-NO cross sections below 3.0 eV. A quantitatively accurate determination of cross sections in this region is difficult since the proper placement of the resonance states relative to the ground state can only be achieved with an elaborate correlated target state and a trial wave function that achieves a balanced description of correlation in the N- and $(N+1)$-electron systems. Moreover, to explain the rich energy structure observed in the cross sections, the nuclear dynamics problem must be solved for all three resonances.

In the present study, we have used the complex Kohn variational method to perform fixed-nuclei electron-NO scattering calculations, in different total symmetries, over a range of internuclear geometries. These calculations provide background elastic cross sections and, in the resonant symmetries, are used to extract the *R*-dependent resonance energies and lifetimes which form the basis for a study of the nuclear dynamics. We have also carried out large-scale coupled-cluster calculations on neutral NO and on the $^3\Sigma^-$, $^1\Delta$ and $^1\Sigma^+$ anion states, at geometries where the latter are electronically bound. We have devised a procedure for analytically continuing these results to geometries where they are electronically unbound, to provide an independent estimate of the complex potential energy curves of the anion states. Finally, we use the local complex potential (LCP) or "boomerang" model [13] to study resonant nuclear dynamics on the different anion curves and to evaluate the vibrational excitation cross sections. Our theoretical results will be shown to capture the essential features of recent experiments, but also suggest the need for a nonlocal treatment of the nuclear dynamics to produce quantitative predictions and to reproduce some features of the cross sections for excitation of higher vibrational levels.

The theoretical formulation we have used is described in the following section. Section III presents the computational details of the present theoretical study. Our results are pre-

sented in Sec. IV, along with comparisons to recent experimental data. We conclude with a brief discussion.

II. THEORETICAL FORMULATION

To understand the general features of low-energy electron-NO scattering, we can use a simple molecular orbital picture of the relevant wave functions. Neutral NO has an open-shell $^2\Pi$ ground state; its electronic configuration is $(\text{core})^8(5\,\sigma)^2(1\,\pi)^4(2\,\pi)^1$. The quasibound (resonance) anion states have the configuration $(\text{core})^8(5\,\sigma)^2(1\,\pi)^4(2\,\pi)^2$. The two open-shell $2\,\pi$ electrons can be coupled to form three states with symmetries $^3\Sigma^-$, $^1\Delta$, or $^1\Sigma^+$, which, by analogy with O_2, are expected to be separated by only a few electron volts. Fixed-nuclei electron-NO scattering in these overall symmetries, at low energies, produces amplitudes (T matrices) that display a prominent resonant behavior that depends strongly on the internuclear separation. The vibrational excitation cross sections are found to be dominated by these resonance contributions. For the vibrationally elastic and total scattering cross sections at low energies, we would expect there to be, in addition to resonance contributions, significant background contributions arising from the $(2\pi\, k\sigma)$ $^1\Pi$ and $^3\Pi$ symmetry components; these components vary slowly with internuclear distance. Fixed-nuclei scattering calculations at the equilibrium geometry should therefore yield accurate values for the background cross sections.

Our approach, then, is to first compute complex potential curves (positions and widths) for the three anion states. We have tackled this problem in two different ways. One approach is to perform fixed-nuclei scattering calculations in the three resonant symmetries and to extract resonance parameters, for each geometry of interest, by analyzing the energy dependence of the eigenphase sums. Since the quality of the electronic wave functions that can realistically be employed in such an approach is limited, relative to what can be achieved in a bound-state calculation, we seek an independent method for computing the resonance parameters. Such a method involves analytic continuation of bound-state results and will be described below.

To evaluate the resonant vibrational excitation cross sections, we have employed the local complex potential model, described briefly below. Since the resonances belong to different total symmetries, the LCP calculations can be carried out seperately for each resonance and these cross sections can be added, with appropriate statistical weights, to produce the physically observed cross sections.

A. Local complex potential model

Traditional approaches to resonant vibrational excitation of molecules by electron impact are generally based on rigorous resonance scattering theory, formulated within the Born-Oppenheimer approximation. The theory can be equivalently formulated in several ways to derive a so-called nuclear wave equation that governs the nuclear dynamics due to the resonance state(s). Following O'Malley [14], who developed the formal theory using the Feshbach formalism [15], we can write the governing equation (for a diatomic target) as

$$\begin{aligned}[E - E_{\text{res}}(R) - K_R]\xi_{\nu_i}(\mathbf{R}) \\ - \lim_{\epsilon\to 0}\sum_{\nu}\int dE' \frac{U_{E'\nu}(\mathbf{R})}{E + i\epsilon - E'}\int d\mathbf{R}' U_{E'\nu}(\mathbf{R}')\xi_{\nu_i}(\mathbf{R}') \\ = U_{E\nu_i}(\mathbf{R}),\end{aligned} \tag{1}$$

where E is the total energy, R is the internuclear distance, K_R is the nuclear kinetic energy operator, $E_{\text{res}}(R)$ is the electronic resonance energy and $\xi_{\nu_i}(\mathbf{R})$ is the wave function, associated with an initial target state having energy E_{ν_i}, that describes the relative motion of the nuclei. The function $U_{E\nu_i}(\mathbf{R})$ is a matrix element of the Hamiltonian between the electronic resonance wave function, $\psi_{\text{res}}(\mathbf{r};\mathbf{R})$, and a background function that describes the nonresonant scattering. If we assume the Born-Oppenheimer approximation to be valid for describing the latter, then $U_{E\nu_i}(\mathbf{R})$ can be factored as

$$\begin{aligned}U_{E\nu}(\mathbf{R}) &= \{\psi_{res}(\mathbf{r};\mathbf{R})|H_{el}(\mathbf{r};\mathbf{R})|\psi_{k_\nu}(\mathbf{r};\mathbf{R})\}\,\eta_\nu(\mathbf{R}) \\ &\equiv \gamma(k_\nu,\mathbf{R})\,\eta_\nu(\mathbf{R}),\end{aligned} \tag{2}$$

where $\psi_{k_\nu}(\mathbf{r};\mathbf{R})$ is the electronic part of the background function and the curly brackets in the first line of Eq. (2) indicate integration over electronic coordinates ($\mathbf{r}$) only and $\eta_\nu(\mathbf{R})$ is a vibrational wave function of the neutral target. k_ν is the channel electron momentum and is defined by energy conservation, $2E = 2E_\nu + k_\nu^2$. Thus the nuclear wave equation of formal resonance theory is an inhomogeneous Schrödinger equation with an effective Hamiltonian that is complex, nonlocal and energy dependent.

Numerical solutions of the nuclear wave equation, at least for diatomic targets, have become routine with current computational methods [16]. The more formidable challenge, with *ab initio* methods, is calculating the parameters that define the nonlocal effective nuclear potential. In particular, the coupling term, $U_{E\nu}(\mathbf{R})$, requires computing a matrix element between a nonresonant scattering function and the electronic resonance wave function. If one uses the formally exact definition of the latter, defined by the residue of the Green's function at a resonance pole [17], then one is necessarily required to perform fixed-nuclei calculations at complex energies to locate the resonance energies, and the coupling matrix elements must generally be defined by analytic continuation from the lower half plane [18]. Alternatively, one could approximate the resonance wave function by a discrete, normalizable function and introduce projection operators to compute the background function, defining the coupling element as an "off-shell" matrix element between the resonance function and the background function [19]. It is worth noting that, in all recent theoretical studies using the nonlocal formalism, an assumed functional form for the coupling matrix element is employed.

In this initial study, we have instead adopted the usual practice of approximating the effective nuclear Hamiltonian by a simpler local operator. These approximations, and the

conditions under which they are justified, are well understood [20,21]. They yield the so-called local complex potential or boomerang equation [13]

$$[E - K_R - E_{\rm res}(R) + i\Gamma(R)/2]\xi_\nu(R) = \phi_\nu(R), \tag{3}$$

where the negative ion potential energy curve is characterized by a real part $E_{\rm res}(R)$ and an imaginary part $-i\Gamma(R)/2$. The "entry amplitude" ϕ_ν is defined as

$$\phi_\nu(r) = (\Gamma(R)/2\pi)^{1/2}\eta_\nu(R), \tag{4}$$

where η_ν is the initial vibrational wave function of the neutral target. The resonant T matrix for vibrational excitation is obtained by projecting the solution of Eq. (3) onto the "exit amplitude" $\phi_{\nu'}$,

$$T_{\nu\nu'}(E) = \langle\phi_{\nu'}|\xi_\nu\rangle. \tag{5}$$

Combining Eqs. (3) and (5) allows us to write $T_{\nu\nu'}(E)$ as the matrix element of a nuclear Green's function between entry and exit amplitudes

$$T_{\nu\nu'}(E) = \langle\phi_{\nu'}|\frac{1}{E - K_R - E_{\rm res}(R) + i\Gamma(R)/2}|\phi_\nu\rangle. \tag{6}$$

The entry and exit amplitudes, ϕ_ν and $\phi_{\nu'}$, depend on the initial and final target vibrational wave functions, but not explicitly on the initial and final electron momenta. This is so because in deriving the boomerang equation, the electron momentum, k_ν, is replaced by the local momentum $k(R)$ at which the resonance would occur if electrons were scattered by molecules with the nuclei fixed at separation R, that is,

$$\frac{k^2(R)}{2} = E_{\rm res}(R) - E_0(R), \tag{7}$$

where $E_0(R)$ is the electronic energy of the target. This approximation is a good one when the resonance energy is much larger than the spacing between the target vibrational levels; in such cases, the local complex potential model can be expected to yield accurate results. In general, the cross sections computed with the boomerang model, which are given by the expression

$$\sigma_{\nu\to\nu'} = \frac{2\pi^3}{E}|T_{\nu\nu'}(E)|^2 \tag{8}$$

will be inaccurate at very low energies and will not have the correct energy dependence near threhold. This problem is sometimes addressed by the *ad hoc* introduction of "barrier penetration factors" [22] into the entry and exit amplitudes that ensure the correct energy behavior of the cross sections near threshold,

$$\phi_\nu(r) = \frac{f(k_\nu)}{f(k(R))}[\Gamma(R)/2\pi]^{1/2}\eta_\nu(R). \tag{9}$$

For example, Wigner's threshold laws can be satisfied by choosing $f(k)$ to be $k^{l+1/2}$, where l is the lowest partial wave that contributes to the resonance. As well as correcting the qualitative behavior at low energies, these somewhat arbitrary factors can significantly change the magnitude of the cross sections away from threshold, so we have not investigated their use in this work.

To compare with physically observed integrated cross sections, the unweighted cross sections for each resonance state, computed with the local complex potential model using Eq. (8), must be multiplied by their appropriate statistical weights and added. For the case of NO, which has a $^2\Pi$ ground state, the physical cross sections are given by the expression

$$\sigma^{\rm total}_{\nu\to\nu'} = \frac{1}{8}(3\sigma^{^3\Sigma^-}_{\nu\to\nu'} + 2\sigma^{^1\Delta}_{\nu\to\nu'} + \sigma^{^1\Sigma^+}_{\nu\to\nu'}). \tag{10}$$

B. Fixed-nuclei electron scattering calculations

The fixed-nuclei electron scattering cross sections were computed using the complex Kohn variational method [23]. In this method, the electronic trial wave function of the scattering system is expanded as

$$\Psi = \sum_\Gamma A[\Phi_\Gamma(x_1,...,x_N)F_\Gamma(x_{N+1})] + \sum_\mu d_\mu\Theta_\mu(x_1,...,x_{N+1}), \tag{11}$$

where the Φ_Γ are N-electron target eigenstates, x_i denote space-spin coordinates, $\mathcal{A}$ antisymmetrizes the coordinates of the target and scattered electrons and the Θ_μ are square-integrable $(N+1)$-electron configuration state functions (CSFs) described further below. The first sum, which we denote as the P-space portion of the wave function, runs over the energetically open target states. We denote the second sum as the correlation portion of the wave function.

In the Kohn method, the F_Γ, which represent the wave functions of the scattered electron, are expanded as a linear combination of symmetry-adapted molecular orbitals (Gaussians) and numerical continuum functions. Although the present study is confined to electronically elastic scattering, the first term in the trial function is written as a sum to reflect the fact that the open-shell ground state of NO is a $^2\Pi$ state and in general, depending on the total symmetry under consideration, both spatial components of the target ground state must be retained in the trial function. The $N+1$-electron CSFs describe short-range correlations and the effects of closed channels and are critical to striking a proper balance between intra-target electron correlation and correlation between target and scattered electrons.

For the target ground state, we use a multiconfiguration wave function obtained by defining a complete active space of molecular orbitals and performing a full configuration-interaction (CI) calculation within that space of orbitals. For the correlation part of the wave function, we included two classes of terms. The first class is the set of all $N+1$-electron CSFs that can be formed from the active space of target orbitals. These are generally referred to as "penetration terms" [23]. Since the scattering functions F_Γ are constucted from bound and continuum functions which are, by construction, orthogonal to the target orbitals, the penetration terms are needed to relax any constraints implied by this strong orthogonality. In addition to the penetration terms, we in-

cluded a second class of "CI relaxation terms" [23]. The target ground state is built as a fixed linear combination of a number of CSFs, say M, from the active space. The target CI calculation can also produce $(M-1)$ excited states, which are presumed to be energetically closed. The CI relaxation terms are constructed as the direct product of these states and the orbitals used to describe the scattered electron. In other words, this class of CI relaxation terms is simply the complement $(1-P)$ of the P-space portion of the wave function. This complement, combined with the penetration terms, constitute the correlation part of the trial wave function. In solving the variational equations, we use Feshbach partitioning to combine the penetration and relaxation terms into an optical potential. For more details on this subject, we refer the reader to Ref. [23].

C. Resonance curves from electronic structure calculations

In addition to performing fixed-nuclei scattering calculations, we have also carried out electronic structure calculations for the NO ground state and the $^3\Sigma^-$, $^1\Delta$ and $^1\Sigma^+$ anion states, in the regions where they are electronically bound, using coupled-cluster methods. We have devised a method for analytically continuing these results to provide complex potential curves in the regions where the anion curves are unbound. In addition to providing a check on the accuracy of the resonance widths extracted from the scattering calculations, this procedure allows us to construct resonance curves with wave functions that include more correlation effects than could realistically be used in any practical scattering calculation.

Consider a bound anion potential curve in a region where it is close to crossing the neutral curve. To the right of the crossing, the R-dependent binding energy, $E_0(R)-E_{\rm res}(R)$, is a positive real number, which we denote as $k(R)^2/2$. To the left of the crossing, $k(R)$ becomes a complex number that characterizes the resonance. We now make an analogy with potential scattering and assume the problem can be described by a Jost function, $\mathcal{F}_l(p(R))$, that describes a scattered electron with momentum $p(R)$ and angular momentum ℓ. For a nonpolar target, we can take ℓ to be the dominant angular momentum component of the resonance. For a polar target, this definition may be modified to incorporate the long-range electron-dipole interaction [24].

Bound states, as well as resonances, correspond to zeros of the Jost function. So the "resonance momentum," $k(R)$, is simply that value of $p(R)$ for which the Jost function vanishes,

$$\mathcal{F}_l(p(R))\big|_{p(R)=k(R)}=0. \tag{12}$$

But near $p(R)=0$, $\mathcal{F}_\ell(p(R))$ can be expanded as [25]

$$\mathcal{F}_\ell(p(R)) = a_0(R)+a_1(R)p(R)^2+\cdots+b_1(R)p(R)^{2\ell+1} + b_2(R)p(R)^{2\ell+3}+\cdots, \tag{13}$$

so what we seek are solutions to the equation

$$0 = a_0(R)+a_1(R)k(R)^2+\cdots+b_1(R)k(R)^{2l+1}+b_2(R)k(R)^{2l+3} +\cdots. \tag{14}$$

The coefficients, $[a_i,b_i]$, can themselves be expanded in a power series in the internuclear distance. So retaining the first three terms in Eq. (13) and expanding the coefficients through first order in R, the equation that defines the resonance curve can be written as

$$0 = 1+c_1R+c_2k(R)^2+c_3Rk(R)^2+c_4k(R)^{2l+1}+c_5Rk(R)^{2l+1}. \tag{15}$$

The known quantities are the real k values and corresponding internuclear distances R where the anion is bound. The unknown coefficients c_i can be determined from these known values by using, for example, a linear least-squares procedure. Having determined these coefficients, we have (for integer ℓ) a polynomial in k whose zeros define the resonance curve for all R. The zeroes of this polynomial will in general be complex and the anion potential curve is defined as $E_0(R)-k(R)^2/2$. As we will see below, this remarkably simple procedure can give very accurate results.

III. COMPUTATIONS

A. Complex Kohn variational scattering calculations

The basis sets for the complex Kohn calculations were chosen as follows. The target orbitals were determined using a basis of contracted Gaussian functions centered on each atom. For oxygen, we used a $(10s6p4d/6s5p4d)$ set which is the same as the $(11s7p4d)$ set described by Gil *et al.* [26], with the most diffuse s and p functions deleted. For nitrogen, we used Dunning's [27] $(9s5p1d/5s3p1d)$ basis. For the scattering calculations, the oxygen basis was augmented with one additional s-type and one additional p type function (exponents 0.0316 for s and 0.0254 for p), while two additional d-type functions (exponents 1.0 and 0.05) were included on the nitrogen.

The target state wave function was obtained from a complete active space configuration-interaction (CASCI) calculation where the active space consisted of 5σ, 6σ, 1π, and 2π orbitals, which yields 54-term functions for each component of the $^2\Pi$ ground state. The target molecular orbitals for these calculations were obtained by first performing a self-consistent field (SCF) calculation on the closed-shell ground state of NO^+. The occupied and virtual molecular orbitals from this calculation were then used to perform a CI calculation for the ground state using a single reference plus all single excitations. The density matrix for this state was diagonalized to produce the 5σ, 6σ, 1π, and 2π natural orbitals for the CASCI calculations that describe the target in the Kohn trial function in $^1\Pi$ and $^3\Pi$ symmetry.

For the symmetries in which negative ion shape resonances occur, we found it necessary to take both the anion states and the neutral ground state into account in determining the active space of target orbitals, so as to get a proper description of the resonance states relative to the NO ground state. For the resonance symmetries, therefore, we also carried out single-reference plus all-singles calculations for the

various anion states. The density matrices from the anion calculations were averaged with the neutral ground state density matrices and then diagonalized to obtain the natural orbitals that were used in the complex Kohn calculations in $^3\Sigma^-$, $^1\Delta$, and $^1\Sigma^+$ symmetry. If the neutral ground-state density matrix were used to generate natural orbitals, our limited CASCI calculations would place the neutral NO potential curve too low relative to the anion states. Conversely, using the anion density matrices to generate the natural orbitals over correlates the resonance states relative to the neutral and places them energetically too low. Averaging the density matrices is a convenient expedient for striking a balance between correlation effects in the neutral and anion states.

The averaging scheme used depends on the symmetry under consideration. In $^3\Sigma^-$ symmetry, we averaged the density matrix for the $^3\Sigma^-$ anion state with the density matrices for the two degenerate components of the $^2\Pi$ ground state. As we will see below, this choice of molecular orbitals gives a good balance between correlation effects in the negative ion state and the neutral ground state in the trial wave function for the scattering calculations. The anion states all have a dominant $2\pi^2$ structure. In $^3\Sigma^-$ symmetry, the two 2π electrons occupy orbitals of *different* spatial symmetry and, consequently, optimal 2π orbitals for the neutral and $^3\Sigma^-$ anion states are rather similar. In the case of the $^1\Delta$ resonance, the two 2π electrons are in the *same* spatial orbital, so the differences between target and anion orbitals are expected to be larger. It is consequently more difficult to describe the neutral and $^1\Delta$ anion states with a common set of active orbitals and we should therefore expect larger errors in that case.

Similar considerations come into play in determining the $^1\Sigma^+$ resonance, despite the fact that the two 2π electrons in that case occupy different spatial orbitals, for reasons that are a bit more subtle. The $^1\Delta$ anion state is doubly degenerate. In the reduced symmetry C_{2v} in which these calculations were performed, one component of the $^1\Delta$ state appears in $^1A_2$ symmetry, the other in $^1A_1$ symmetry. The $^1\Sigma^+$ resonance also appears in $^1A_1$ symmetry. The contributions to the total cross section from $^1\Delta$ and $^1\Sigma^+$ symmetry are strictly additive: the $^1\Delta$ and $^1\Sigma^+$ resonance contributions to the cross section in $^1A_1$ symmetry overlap, but they do not interfere. In order to extract the resonance parameters for the $^1\Sigma^+$ anion state from a calculation performed in $^1A_1$ symmetry, we must first subtract the contribution from the $^1\Delta$ resonance. The latter can be obtained unambiguously from the calculations performed in $^1A_2$ symmetry. For the subtraction procedure to work, we must assure that the two components of the $^1\Delta$ state remain strictly degenerate. This means that the active orbitals used in both $^1\Delta$ and $^1\Sigma^+$ symmetry calculations must be chosen identically. The averaging scheme we used in these symmetries therefore included the density matrices for the neutral ground state and both the $^1\Delta$ and $^1\Sigma^+$ anion states.

As outlined in Sec. II B, the complex Kohn trial function included all CSFs generated by placing eight electrons in the four frozen core orbitals, seven electrons in the active space and one electron in the (augmented) virtual space. This set plus the remaining penetration terms gave trial functions of $\sim$5000 configurations for each total symmetry considered. For the resonant $^3\Sigma^-$, $^1\Delta$, and $^1\Sigma^+$ symmetries, calculations were performed over a range of internuclear distances and the resonance parameters extracted by fitting the eigenphase sums to a Breit-Wigner form. For geometries where the negative ion states become electronically bound, i.e., where they lie below the neutral NO ground state, their energies were determined by diagonalizing the "bound" portion of the full Kohn Hamiltonian.

TABLE I. Resonance parameters for the three low-lying NO^- states at an internuclear separation of 2.1747 bohr.

Symmetry	E_{res} (hartree)	Γ_{res} (hartree)	Model
$^3\Sigma^-$	0.017	0.0064	Analytic continuation
	0.016	0.0060	Complex Kohn
	0.033	0.0065	Ref. [10]
	0.017		Ref. [9]
$^1\Delta$	0.057	0.036	Analytic continuation
	0.045	0.031	Complex Kohn
	0.066	0.027	Ref. [10]
	0.042		Ref. [9]
$^1\Sigma^+$	0.076	0.062	Complex Kohn
	0.098	0.045	Ref. [10]

Table I lists the resonance parameters we obtained from these calculations at the equilibrium internuclear separation of the target. For comparison, we have listed the values obtained by Tennyson and Noble in their one-state, static-exchange plus polarization *R*-matrix calculations. These authors also reported results for six-state *R*-matrix calculations, but those results evidently led to an unbalanced description of the anion states, since the $^3\Sigma^-$ anion state appeared bound relative to the ground state of NO in those calculations. Also listed in Table I are the resonance energies for the $^3\Sigma^-$ and $^1\Delta$ states obtained by Teillet-Billy and Fiquet-Fayard [9] from a semiempirical analysis of the experimental data of Tronc *et al.* [4].

For the background $^1\Pi$ and $^3\Pi$ symmetries, we only performed calculations at the equilibrium internuclear separation of 2.1747 bohr. The eigenphase sums and integrated cross sections for these symmetries are plotted as a function of energy in Fig. 1. The only other theoretical data available for comparison in this energy range are the eigenphase sums reported by Tennyson and Noble [10] using the *R*-matrix method, which are rather different from the present results. The *R*-matrix calculations included polarization effects but, unlike the present calculations, they employed an SCF target wave function.

B. Coupled-cluster calculations

We also carried out electronic structure calculations using the coupled-cluster (CC) method. We performed coupled-cluster, single- and double-excitation calculations with a noniterative triples correction (CCSD(T)) [28] using augmented, correlation-consistent, polarized valence triple-zeta basis sets [29,30] on the neutral target and negative ion states. The CC calculations give unambiguous values for the anion potential energy curves at geometries where they are electronically bound. To the left of their respective crossings

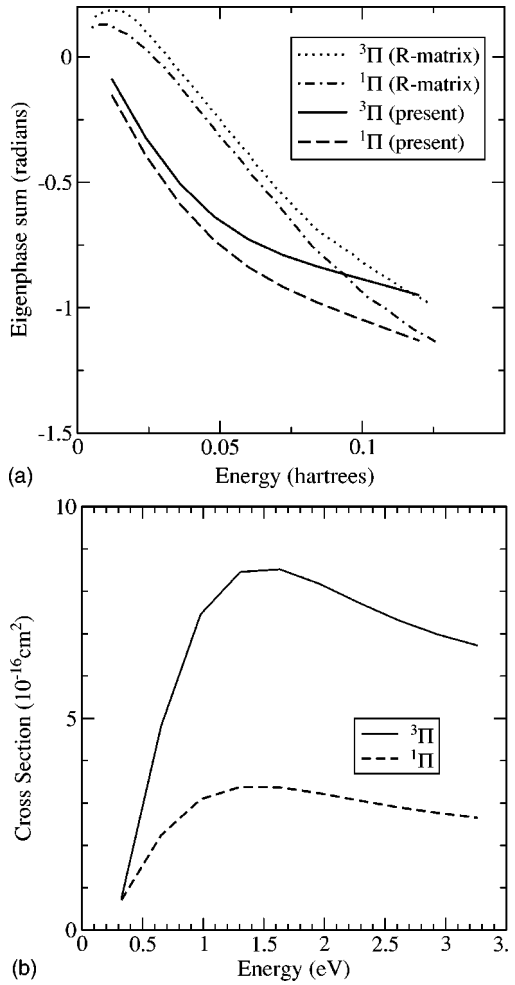

FIG. 1. Eigenphase sums, in radians, and integrated fixed-nuclei cross sections, in atomic units ($1a_0^2 = 0.28 \times 10^{-16}$ cm^2) for e^--NO scattering in $^3\Pi$ and $^1\Pi$ symmetry at equilibrium geometry. The *R*-matrix results are from Ref. [10]. The cross sections include statistical weights of 1/4 and 3/4 for the $^1\Pi$ and $^3\Pi$ cases, respectively.

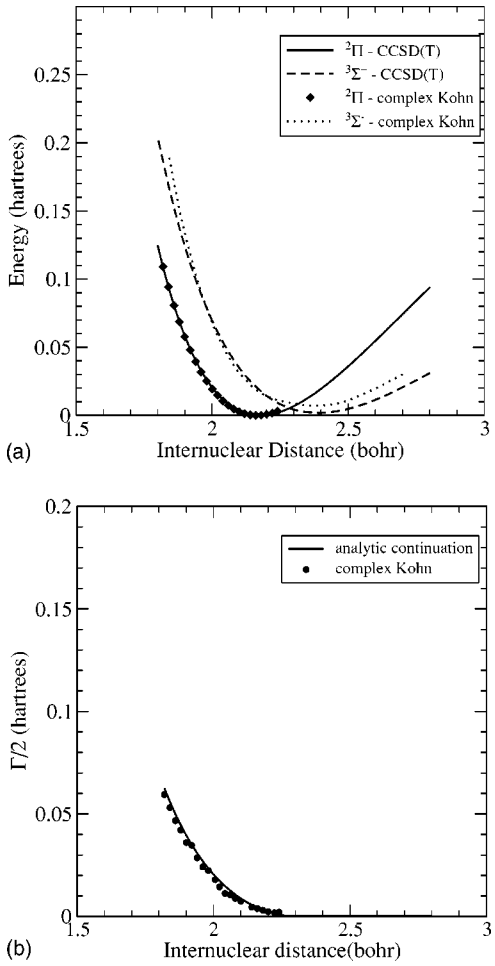

FIG. 2. Comparison of $^3\Sigma^-$ resonance energies and widths from complex Kohn and electronic structure calculations. Upper panel: NO ground state and real part of the $^3\Sigma^-$ resonance energies. The portion of the CCSD(T) resonance curve to the left of its crossing with the neutral curve was obtained by analytic continuation. Lower panel: resonance widths.

with the ground state NO curve, the anion states become complex quantities. For these latter geometries, we carried out analytic continuations for each anion state using the procedure outlined in Sec. II C. For the angular momentum of the resonantly scattered electron, we used the value $\ell = 1$. As previously mentioned, one can modify this choice in the case of a polar target to take account of *R*-dependent dipole moment [24,31]. We found this modification to be negligible (less than 1%) in the present case, since the dipole moment of NO is small (0.15 D) at equilibrium and goes through zero over the Franck-Condon region of interest here.

C. Complex resonance curves

The resonance energies and widths from both the complex Kohn calculations and CC calculations are plotted in Figs. 2–4. Note that all energies are plotted relative to the minimum of the NO ground state, which is taken as the zero of energy. For the $^3\Sigma^-$ anion case, the complex Kohn and the analytic continuation model give virtually identical resonance parameters, giving us additional confidence in the validity of the Jost function model, as well as in the accuracy of the variational scattering results for this symmetry.

For the $^1\Delta$ case, the agreement is not quite as good as in the $^3\Sigma^-$ case. We believe the complex Kohn results to be less accurate in this case, reflecting the fact, as stated earlier, that it is more difficult to describe the neutral and negative ion states with a common set of molecular orbitals in this case. Nevertheless, the resonance widths for the $^1\Delta$ state obtained from the scattering calculations and from analytic continuation are seen to be very similar.

The results for the third resonance, $^1\Sigma^+$, are shown in Fig. 4. We see from the coupled-cluster results for this case that the negative ion curve remains very close to the neutral curve to the right of their crossing near 2.9 bohr. To understand this behavior, it is again useful to point to the analogy between the NO^- states and the states of O_2. In the case of oxygen, the $^3\Sigma_g^-$, $^1\Delta$ and $^1\Sigma_g^+$ states all dissociate to $O(^3P) + O^-(^2P)$. However, in the case of NO^-, as Zecca [3] pointed out, only the $^3\Sigma^-$ dissociates to $N(^4S) + O^-(^2P)$. The $^1\Delta$ and $^1\Sigma^+$ states both correlate with $N^-(^3P) + O(^3P)$. But the electron affinity

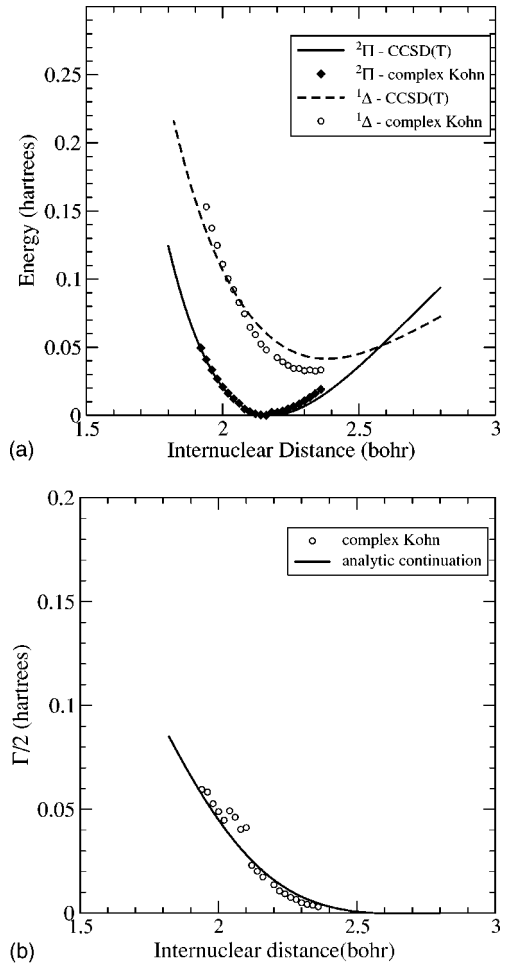

FIG. 3. As in Fig. 2, for the $^1\Delta$ resonance.

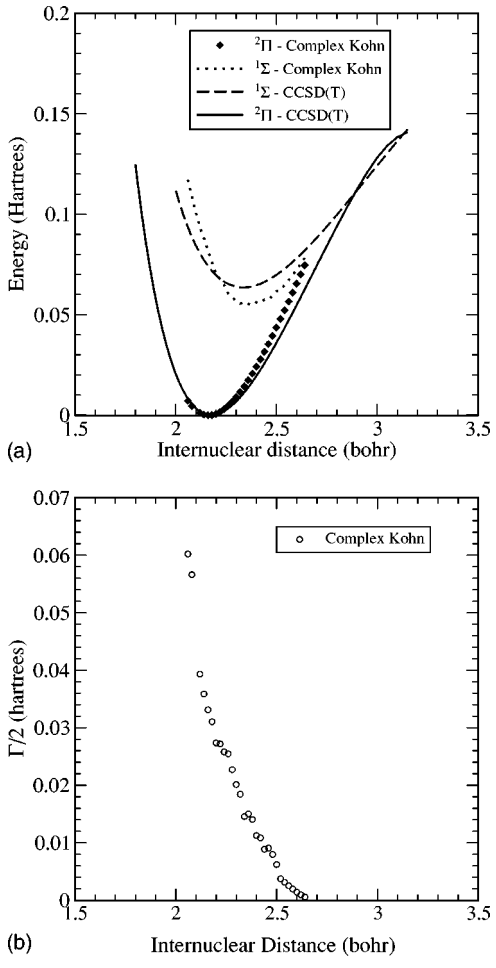

FIG. 4. As in Fig. 2, for the $^1\Sigma^+$ resonance. Note that the CCSD(T) $^1\Sigma^+$ curve in the upper panel is the raw result, not the analytically continued result.

of nitrogen is essentially zero, so the neutral NO curve and the $^1\Delta$ and $^1\Sigma^+$ states must all correlate to the same limit. This behavior is clearly evident for the $^1\Sigma^+$ anion, which crosses the neutral curve at a large R value. Since there is no region where the $^1\Sigma^+$ state is electronically bound and well separated from the neutral ground state, the analytic continuation procedure cannot be carried out for the third resonance. The CC curve to the left of the crossing shown in Fig. 4 is thus the "raw" energy obtained from the structure calculation.

The complex Kohn results for the $^1\Sigma^+$ case show the resonance crossing the neutral at a somewhat smaller internuclear distance than the CC results show. There was also more uncertainty in obtaining the resonance widths in this case, since the $^1\Sigma^+$ resonance becomes quite broad, making a Breit-Wigner analysis difficult. Since we felt that the coupled-cluster results for the $^1\Sigma^+$ state are quite accurate in the vicinity of the crossing with the neutral curve, we used the CC results for the real part on the resonance energy in the local complex potential calculations, along with the widths from the scattering calculations. The R dependence of the widths was shifted by. 0.2 bohr to insure that Γ vanishes at the point where the resonance state crosses the neutral.

IV. RESULTS

The resonance contributions to the integrated vibrational excitation cross sections we obtained using the local complex potential model are shown in Fig. 5. The $^3\Sigma^-$ and $^1\Delta$ cross sections both show pronounced boomerang structures, while the broad $^1\Sigma^+$ resonance gives structureless cross sections that rapidly diminish with increasing final vibrational quantum number. The peaks in the $^3\Sigma^-$ cross sections are narrower than those in the $^1\Delta$ cross sections, reflecting the difference in the widths of the two resonances. In the vibrationally elastic cross sections, the $^1\Delta$ and $^1\Sigma^+$ cross sections both display a qualitatively incorrect dependence on energy below 1 eV, rising rather than falling with decreasing energy. For both cases, this energy range falls well outside the resonance region where the local complex potential model is valid. Moreover, the results shown in Fig. 5 were obtained without including any barrier penetration factors in the boomerang calculations that would force the cross sections to vanish at threshold.

To help explain the structures seen in the computed cross sections, we refer to Fig. 6, which shows the vibrational levels of the $^2\Pi$ neutral and the $^3\Sigma^-$ and $^1\Delta$ anion states, the latter computed using the real parts of the resonance poten-

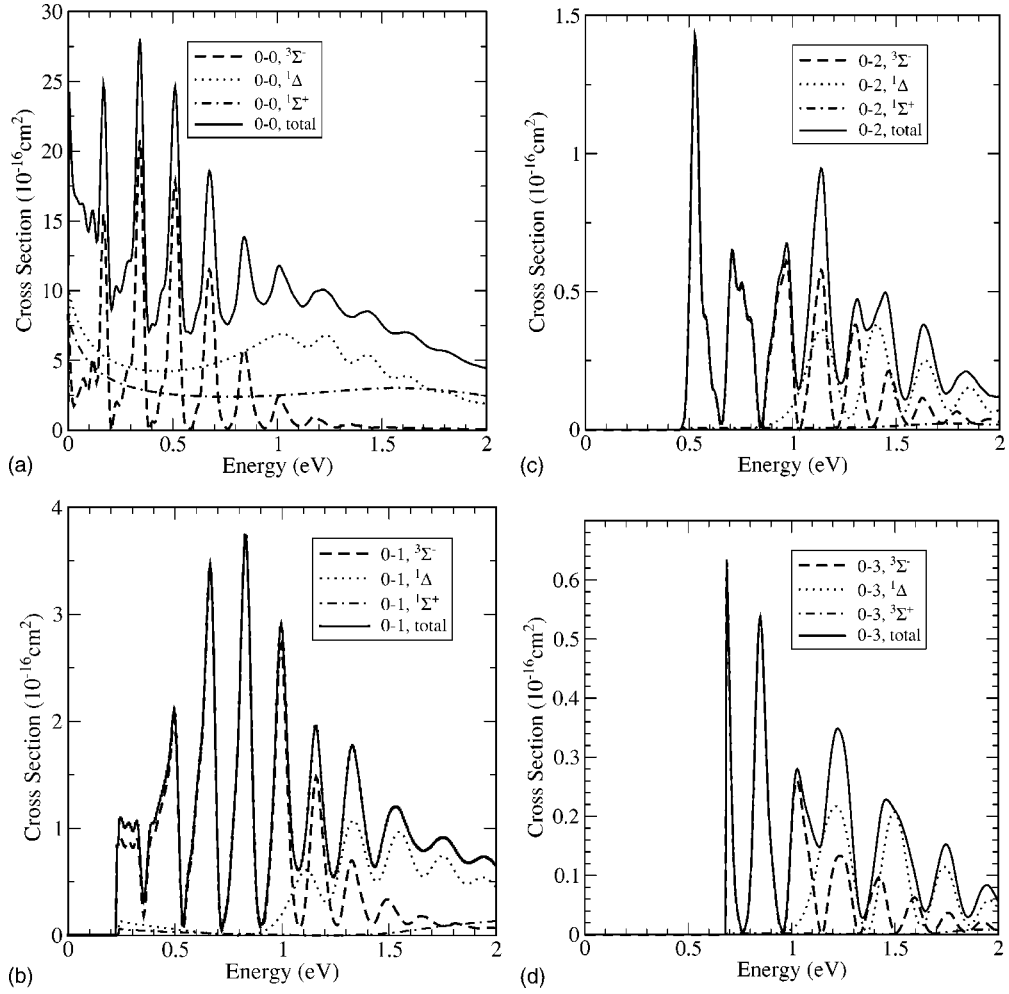

FIG. 5. Local complex potential results for the 0-0, 0-1, 0-2, and 0-3 electron-NO vibrational excitation cross sections. The $^3\Sigma^-$, $^1\Delta$, and $^1\Sigma^+$ symmetry contributions, including statistical weights of 3/8, 1/4, and 1/8, respectively, are shown, as well as the total cross sections.

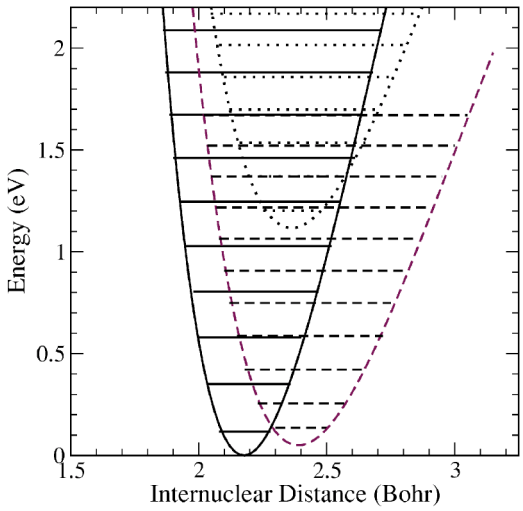

FIG. 6. Neutral and anion potential curves and vibrational levels. Solid curve, ground-state NO curve; dashed curve, $^3\Sigma^-$ anion curve; dotted curve, $^1\Delta$ anion curve.

tial curves. These curves can be compared to the semiempirical curves obtained by Teillet-Billy and Fiquet-Fayard [9] (not shown). The equilibrium internuclear distances for the $^3\Sigma^-$ and $^1\Delta$ anion states we calculated (2.39 and 2.37 bohr, respectively) are very close to the semiempirical values, as are the relative shapes of the curves. Moreover, the energies of the $^3\Sigma^-$ levels we find, relative to those of the neutral, are also close to the semiempirical values. For the $^1\Delta$ anion state, however, our calculations give a curve which lies $\sim$0.35 eV above the one determined semiempirically. Teillet-Billy and Fiquet-Fayard's analysis of the data of Tronc *et al.* [4] assumed a coincidence of the $^3\Sigma^-(\nu=7)$ and $^1\Delta(\nu=2)$ levels as a criteria to position the $^1\Delta$ curve relative to the $^3\Sigma$ curve. Our calculations, on the other hand, show the $^3\Sigma^-(\nu=8)$ and $^1\Delta(\nu=1)$ levels to coincide in energy.

Inspection of the $^3\Sigma^-$ curve shows that its lowest vibrational level lies outside the Franck-Condon region of the neutral ground level and hence makes no contribution to any of the cross sections. The progression of peaks seen in the elastic $(0-0)$ $^3\Sigma^-$ cross section, starting near 0.1 eV, arise from the $\nu=1,2,3\ldots$ vibrational levels of the anion. For the case of $0-1$ excitation, the $\nu=1$ level of the $^3\Sigma^-$ anion is energetically closed, so the progression of observed peaks

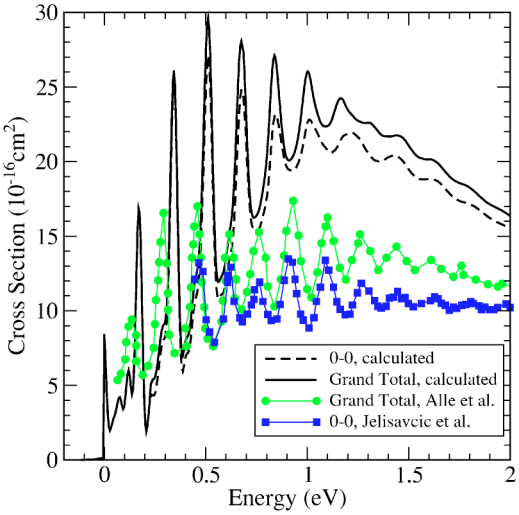

FIG. 7. Comparison of theory and experiment for vibrationally elastic and grand total cross sections.

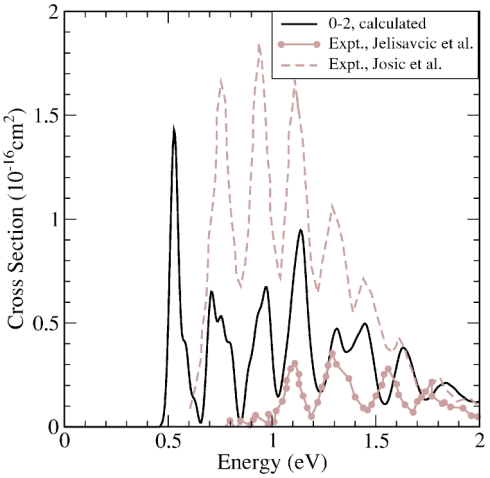

FIG. 9. Comparison of theory and experiment for the 0-2 cross section.

begins with $\nu=2$ anion level. Analogously, the peaks in the 0–2 and 0–3 $^3\Sigma^-$ cross sections arise from the $\nu=4,5...$ and $\nu=5,6...$ anion levels, respectively. It is also worth noting that, in $^3\Sigma^-$ symmetry, the energy location of a given peak does not change when observed in different exit channels.

In the case of the $^1\Delta$ cross sections, the $\nu=0$ anion level is again Franck-Condon forbidden, so the progression of peaks observed in all the cross sections corresponds to resonance contributions arising from the $\nu=1,2,3...$ anion levels. In this case, however, the peak positions are not constant with respect to exit channel quantum number, shifting to higher energy as the excitation level increases. The peaks are also seen to broaden with increasing excitation. These features are both associated with the shorter lifetime (larger width) of the $^1\Delta$ anion, relative to the $^3\Sigma^-$ state.

Our calculated cross sections are compared with experiment in Figs. 7–9. The integrated elastic and total cross sections are shown in Fig. 7. For reference, our calculated grand total cross sections (the sum of the integrated elastic and vibrationally inelastic cross sections) are also tabulated in Table II. The authors will provide tabulated values for other cross sections upon request. The calculated results for the integrated elastic cross section were obtained by adding the background $^{1,3}\Pi$ (Fig. 1) cross sections to the resonance cross section [Eq. (10)]. We also adjusted the $^1\Delta$ and $^1\Sigma^+$ contributions to the 0-0 cross sections (Fig. 5) below 1 eV so that they go smoothly to zero. The experimental results for the total cross section are those of Alle, Brunger, and Buckman [5], obtained by high resolution time-of-flight spectroscopy, while the integrated elastic results plotted are the recent absolute crossed-beam measurements of Jelisavcic, Panajotovic, and Buckman [7]. The recent results of Josic *et al.* (not shown) [6] — obtained from a semiempirical analysis using measured electron-swarm data—give total cross sections very close to those of Alle and co-workers. The calculated cross sections are seen to be ~40% larger than the measured values, but are qualitatively very similar, showing a pronounced series of resonance peaks superimposed on a rising background cross section. The peak spacings and widths are in reasonably good accord with experiment.

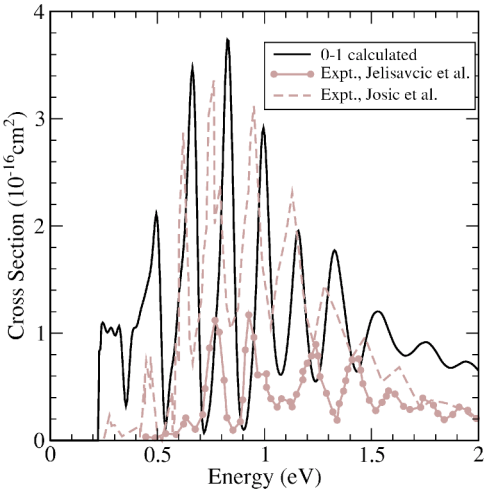

FIG. 8. Comparison of theory and experiment for the 0-1 cross section.

The 0-1 integrated vibrational excitation cross sections are presented in Fig. 8. For comparison, we show the calculated results, the crossed-beam results of Jelisavcic, Panajotovic and Buckman [7] and the swarm-derived results of Josic *et al.* [6]. In magnitude, our results are closer to those of Josic *et al.*. When compared with the direct crossed-beam measurements, however, there are significant qualitative differences. While the calculated results show a progression of peaks arising from the $^3\Sigma^-$ resonance (see Fig. 5), only two low-energy narrow peaks are seen experimentally. The peaks arising from higher vibrational levels of the $^3\Sigma^-$ anion, while prominent in the measured elastic cross section, are evidently suppressed in the excitation cross section. In the swarm-derived results, the peak positions for all the excitation cross sections were fixed to coincide with those measured by Alle, Brunger and Buckman for the total cross section.

The 0-2 vibrational excitation cross sections are plotted in Fig. 9. In this case, our calculated cross sections fall between the crossed-beam and swarm-derived results in magnitude,

TABLE II. Calculated e^--NO grand total cross sections (TCS) as a function of energy. Cross sections are in units of $10-16$ cm^2 and energies are in eV.

Energy	TCS	Energy	TCS	Energy	TCS
0.0	8.437	0.364	14.184	0.800	20.198
0.011	4.842	0.370	10.683	0.816	23.720
0.027	1.968	0.375	8.305	0.832	26.840
0.044	2.706	0.380	7.156	0.838	27.115
0.049	2.915	0.386	6.976	0.859	24.636
0.071	4.148	0.402	8.069	0.881	21.401
0.076	4.207	0.413	8.354	0.897	20.251
0.092	3.414	0.429	9.923	0.908	20.074
0.097	3.572	0.446	11.985	0.919	20.155
0.114	5.770	0.462	13.183	0.936	20.558
0.119	6.013	0.478	17.341	0.952	21.456
0.125	5.644	0.489	22.473	0.968	22.982
0.136	4.401	0.495	25.192	0.985	24.939
0.146	6.335	0.506	29.118	1.001	26.038
0.157	12.402	0.522	26.867	1.017	25.342
0.168	16.849	0.527	24.007	1.034	24.084
0.179	14.348	0.533	20.733	1.050	23.212
0.190	7.330	0.538	17.579	1.083	22.364
0.201	2.477	0.544	14.991	1.099	22.382
0.206	1.903	0.549	13.212	1.115	22.629
0.217	3.057	0.555	12.252	1.132	23.265
0.223	3.802	0.560	11.925	1.148	23.942
0.228	5.079	0.571	12.124	1.191	23.665
0.244	5.426	0.587	12.647	1.251	22.723
0.255	5.899	0.604	14.047	1.284	22.576
0.261	6.395	0.620	15.551	1.317	22.528
0.272	7.646	0.636	17.823	1.349	22.014
0.283	8.695	0.642	19.306	1.382	21.698
0.299	9.253	0.647	21.144	1.415	21.690
0.304	9.740	0.658	25.086	1.480	21.458
0.310	10.900	0.669	27.702	1.512	20.809
0.315	12.974	0.674	28.048	1.545	20.318
0.321	15.947	0.685	27.327	1.578	20.161
0.326	19.455	0.702	21.941	1.676	19.378
0.331	22.829	0.712	18.575	1.708	18.897
0.337	25.265	0.723	16.730	1.741	18.614
0.342	26.090	0.729	16.363	1.806	18.186
0.348	24.999	0.734	16.237	1.839	17.798
0.353	22.187	0.745	16.303	1.937	16.870
0.359	18.292	0.772	17.420	2.002	16.322

but the qualitative differences between theory and direct measurement are now more significant. The beam measurements show a complete suppression of the $^3\Sigma^-$ resonance peaks in the 0-2 cross section: while the energy threshold for excitation is 0.46 eV in this case, the beam data show no significant excitation below 1.1 eV.

Jelisavcic and co-workers [7] have suggested that interference between the resonances might be responsible for some of the observed features, but this possibility can be ruled out on theoretical grounds. As pointed out above, the negative ion states all have different total symmetries, so their contributions to the integrated cross sections are strictly additive, even beyond the local complex potential model. The suppression of resonance features in the higher excitation cross sections is more likely a dynamical effect that cannot be described by boomerang model calculations that employ a strictly local potential as well as energy-independent entry and exit amplitudes. The introduction of an energy-modified exit amplitude, as in Eq. (9), into the boomerang model would be one way of (arbitrarily) supressing the near-threshold peaks in the cross sections. It is more likely that a fully nonlocal treatment of the dynamics for the lowest resonance, which we intend to explore in future work, will be required to obtain better agreement with experiment.

V. DISCUSSION

We have presented the results of a fully *ab initio* treatment of electron-NO scattering in the low-energy region dominated by negative ion shape resonances. The fixed-nuclei cross sections were computed using the complex Kohn variational method and were used to extract the required resonance parameters. These parameters were independently checked using large-scale electronic structure calculations along with an analytic continuation scheme we devised for evaluating the resonance widths.

These initial *ab initio* results confirm the interpretation that the prominent features observed in the elastic and vibrational excitation cross sections arise from $^3\Sigma^-$ and $^1\Delta$ negative ion states. The lowest energy peaks observed are due to the $^3\Sigma^-$ state and appear at the same energy in different exit channels. The $^3\Sigma^-$ peaks are overlapped by a broader series of $^1\Delta$ peaks at higher energies which shift in energy as the exit channel quantum number changes. We have also found that the third $^1\Sigma^+$ resonance, which contributes to the elastic background cross section, is too broad to display any boomerang structure.

While the local complex potential model we have used manages to capture essential features of the measured cross sections, there are deficiencies in the treatment that become increasingly apparent in the higher excitation cross sections. The vibrational levels of the $^3\Sigma^-$ anion are energetically close to those of the neutral target, which invalidates several key assumptions used in deriving the local complex potential model [20,21]. Nonlocal effects, beyond the boomerang model, may be critical in explaining the suppression of resonance peaks that occurs in the higher excitation cross sections. We hope to explore these effects in future studies of this interesting and challenging system.

ACKNOWLEDGMENTS

This work was performed under the auspices of the U.S. Department of Energy by the University of California,

Lawrence Berkeley National Laboratory under Contract No. DE-AC03-76SF00098. The work was supported by the U.S. DOE, Office of Basic Energy Science, Division of Chemical Sciences and computations were carried out at the National Energy Research Scientific Computing Center at Lawrence Berkeley National Laboratory. A.E.O. acknowledges support from the National Science Foundation (Grant No. PHY-99-87877).

[1] D. Spence and G. J. Schulz, Phys. Rev. A **3**, 1968 (1971).
[2] P. D. Burow, Chem. Phys. Lett. **26**, 265 (1974).
[3] A. Zecca, I. Lazzizzera, M. Krauss, and C. E. Kuyatt, J. Chem. Phys. **61**, 4560 (1974).
[4] M. Tronc, A. Huetz, M. Landau, F. Pichou, and J. Reinhardt, J. Phys. B **8**, 1160 (1975).
[5] D. T. Alle, M. J. Brunger, and S. J. Buckman, J. Phys. B **29**, L277 (1996).
[6] L. Josic, T. Wroblewski, Z. L. Petrovic, J. Mechlinska-Drewko, and G. P. Karwasz, Chem. Phys. Lett. **350**, 318 (2001).
[7] M. Jelisavcic, R. Panajotovic, and S. J. Buckman, Phys. Rev. Lett. **90**, 203201 (2003).
[8] F. Koike, J. Phys. Soc. Jpn. **39**, 1590 (1975).
[9] D. Teillet-Billy and F. Fiquet-Fayard, J. Phys. B **10**, L111 (1977).
[10] J. Tennyson and C. J. Noble, J. Phys. B **19**, 4025 (1986).
[11] F. J. da Paixao, M. A. P. Lima, and V. McKoy, Phys. Rev. A **53**, 1400 (1996).
[12] M. W. Siegel, R. J. Celotta, J. L. Hall, J. Levine, and R. A. Bennett, Phys. Rev. A **6**, 607 (1972).
[13] D. T. Birtwistle and A. Herzenberg, J. Phys. B **4**, 53 (1971).
[14] T. F. O'Malley, Phys. Rev. **150**, 14 (1966).
[15] H. Feshbach, Ann. Phys. (N.Y.) **19**, 287 (1962).
[16] W. Domcke, Phys. Rep. **208**, 97 (1991).
[17] R. M. More and E. Gerjuoy, Phys. Rev. A **7**, 1288 (1973).
[18] T. N. Rescigno and C. W. McCurdy, Phys. Rev. A **34**, 1882 (1986).
[19] A. U. Hazi, J. Phys. B **11**, L259 (1978).
[20] R. J. Bieniek, J. Phys. B **13**, 4405 (1980).
[21] A. U. Hazi, T. Rescigno, and M. Kurilla, Phys. Rev. A **23**, 1089 (1981).
[22] J. N. Bardsley, in *Electron-Molecule and Photon-Molecule Collisions*, edited by T. Rescigno,V. McKoy, and B. Schneider (Plenum, New York, 1979), p. 267.
[23] T. N. Rescigno, B. H. Lengsfield, and C. W. McCurdy, in *Modern Electronic Structure Theory*, edited by D. R. Yarkony (World Scientific, Singapore, 1995), Vol. 1, p. 501.
[24] W. Vanroose, C. W. McCurdy, and T. N. Rescigno, Phys. Rev. A **68**, 052713 (2003).
[25] R. G. Newton, *Scattering Theory of Particles and Waves*, 2nd ed. (Springer, New York, 1982).
[26] T. J. Gil, T. N. Rescigno, C. W. McCurdy, and B. H. Lengsfield, Phys. Rev. A **49**, 2642 (1994).
[27] T. H. Dunning, J. Chem. Phys. **53**, 2823 (1970).
[28] P. J. Knowles, C. Hampel, and H. Werner, J. Chem. Phys. **99**, 5219 (1993).
[29] T. H. Dunning, J. Chem. Phys. **90**, 1007 (1989).
[30] R. A. Kendall, T. H. Dunning, Jr., and R. J. Harrison, J. Chem. Phys. **96**, 6796 (1992).
[31] M. H. Mittleman and R. E. von Holdt, Phys. Rev. **140**, A726 (1965).